Continental Shelf Research 65 (2013) 81–96

Contents lists available at SciVerse ScienceDirect

Continental Shelf Research

journal homepage: www.elsevier.com/locate/csr

Dynamics of barotropic low-frequency fluctuations in San Francisco Bay during upwelling

S. Sankaranarayanan *, Oliver B. Fringer

Environmental Fluid Mechanics Laboratory, Stanford University, Stanford, CA 94305, USA

ARTICLE INFO

Article history:
Received 1 October 2012
Received in revised form
23 May 2013
Accepted 6 June 2013
Available online 15 June 2013

Keywords:
Hydrodynamic modeling
Low-frequency fluctuations
San Francisco Bay

ABSTRACT

Observations of wind, surface elevations, and currents in San Francisco Bay during the 1999 upwelling season are analyzed to understand the dynamics of low-frequency currents in upwelling-dominated estuaries. Principal component analysis is carried out to distinguish the different uncorrelated components of the low-frequency fluctuations in the observations. Analyses of ADCP observations at two locations in the Bay show that barotropic currents flow in the direction of winds in the shallow parts of the cross section and flow against the wind in the deeper parts of the cross-section. We ran the SUNTANS model with three forcing functions: (i) winds, (ii) low-frequency surface elevations, and (iii) winds and low-frequency surface elevations, to determine the forcing functions that best reproduce the observed low-frequency fluctuations. Analyses of observations and model simulations show that wind-driven flow in the shallow areas and upwind in the deeper areas, consistent with linear theory. Model simulations also show that the low-frequency currents in the Bay generated due to local winds capture the mean low-frequency barotropic fluctuations seen in the observations during the upwelling season. Model simulations showed that the current generated due to the coastal sea level forcing at the mouth of the Bay is small because the coastal sea levels inside the Bay are in phase with that at the mouth and thus generate weak or negligible pressure gradients. We conclude that forcing of low-frequency sea level fluctuations along the offshore boundaries in the model simulations does not lead to improvement in the prediction of low-frequency currents in San Francisco Bay.

1. Introduction

Tidal processes play a dominant role in the exchange of pollutants, biology, salt, heat and sediments between estuaries and the coastal ocean (Fischer et al., 1979). However, subtidal variations over days to months in the ocean climate on the shelf can also play a major role in forcing variations in long-term circulation in estuaries and Bays. In contrast to the known frequencies of tides, low-frequency fluctuations occur at a range of unknown frequencies and are nonstationary. Subtidal fluctuations in sea level and currents in estuaries and coastal embayments are caused by direct action of local winds on the estuary surface and remote action of the winds on the adjacent shelf, through the coastal Ekman effect. The changes in climate patterns such as Pacific Decadal Oscillations (PDO) and North Pacific Gyre Oscillations and the related changes in wind-forcing can modify coastal currents, upwelling, and low-frequency fluctuations in estuaries. Largier (1996) and Hickey and Banas (2003) highlight the importance of low-frequency currents and upwelling on the circulation in San Francisco Bay and Pacific Northwest coastal estuaries, respectively. Cloern et al. (2007) note that large seasonal phytoplankton blooms began occurring in San Francisco Bay in 1999, despite the decreasing nutrient inputs into the Bay during the preceding two decades. The increase in phytoplankton biomass in the Bay coincided with the sharp decline of bivalve mollusks, the key phytoplankton consumers in the estuary. Cloern et al. (2007) attribute the sudden biological community changes in San Francisco Bay over three trophic levels to the changes in the California Current System, characterized by increasing upwelling intensity, amplified primary productivity and fast filtration removal of phytoplankton cells by bivalve mollusks (Cloern, 1996). Through a systematic analysis of 20-year biological observations, Cloern and his colleagues found that the phytoplankton population in the Bay was low during 1978–1997 and that large chunks of inorganic nitrogen and phosphorus were left unused during that period. Cloern et al. (2007) note that the increased phytoplankton masses in San Francisco Bay since 1999 signaled its weakened resistance to phytoplankton blooms. Cloern et al. (2010) studied the effect of climate patterns on the biological community changes in San Francisco Bay during 1990–2010 and showed that populations of fish, crabs and shrimp co-vary with

* Corresponding author. Present address: 472, Madera Avenue, #1, Sunnyvale, CA 94086, USA.
E-mail addresses: sankara68@gmail.com, sankara68@yahoo.com (S. Sankaranarayanan).

0278-4343/$ - see front matter © 2013 Elsevier Ltd.. All rights reserved.
http://dx.doi.org/10.1016/j.csr.2013.06.006

the Pacific Decadal Oscillation (PDO) and the North Pacific Gyre Oscillation (NPGO), both of which reversed signs in 1999. Lorenzo et al. (2008) note that the NPGO is primarily driven by regional and basin-scale variations in wind-driven horizontal advection. Cloern et al. (2010) attributed the simultaneous shifts in climate patterns and community variability in San Francisco Bay to the changes in oceanic wind-forcing that affect coastal currents and upwelling.

Wang and Elliot (1978) studied the effects of winds on the shelf and noted that 20-day fluctuations in sea levels and currents in Chesapeake Bay were caused by changes in coastal sea levels that had been generated by earlier alongshore winds through the Ekman flux. Similarly, Wong and Wilson (1984) found that spatially coherent fluctuations in Great South Bay, Long Island Sound, were forced primarily by alongshore winds through coastal Ekman upwelling dynamics. Wang and Elliot (1978) recommended that open ocean boundary conditions for the estuarine models include the adjacent coastal ocean in order to capture the effects of winds on the shelf. Garvine (1985) used scaling analysis and a simple barotropic model and found that the wavelength of the coastally forced subtidal fluctuations is much longer than the length of the estuaries and so the coastally forced sea levels within the estuary closely follow those at the mouth without any phase lag. Ryan and Noble (2007) found that at least 40% of the subtidal fluctuations in the sea levels in San Francisco Bay are tied to the large scale wind forcing affecting the coastal ocean. Wong (1994) studied the circulation in estuaries with rectangular and triangular cross sections forced with a steadily rising or falling coastal sea level at the mouth to simulate remote forcing. Coastal sea-level setdown at the mouth of a rectangular estuary generates down-

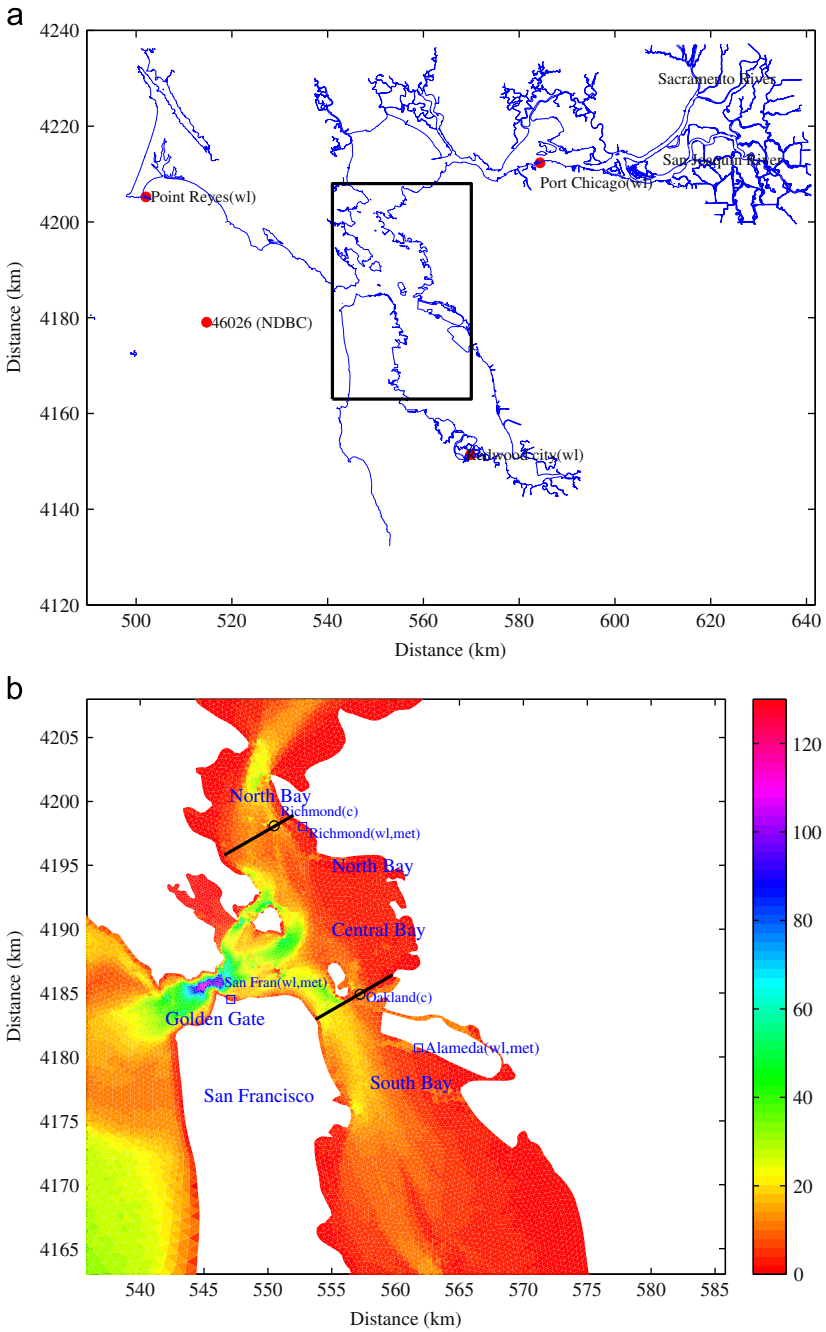

Fig. 1. San Francisco Bay and the adjacent coastal Pacific Ocean (a) and the study area (b) with station locations overlaid over the bathymetry (in m below MSL). Legend: wl, water level; C, ADCP; met, meteorological.

estuary currents with faster currents near the surface. On the other hand, coastal sea-level setdown in a triangular estuary generates faster currents near the deep channels and slower currents near the shore (Wong, 1994).

The currents induced by local winds play a major role in semi-enclosed bays and lagoons. A constant wind stress on the top of a constant depth channel produces a flow that changes in direction with depth. Fischer (1976) showed through laboratory experiments that constant winds blowing over a basin of variable depth induce a vertically averaged mean current flowing with the wind in the shallow channels and against the wind in the deeper channels. A down-estuary wind stress generates a wind-setdown at the head of the estuary due to piling up of water. The flow is downwind in the shallow portion with bottom stress balancing the surface stress and with the pressure gradient playing a minor role. The flow is upwind in the deeper channels where the pressure gradient plays a larger role. The wind-driven circulation can thus be explained as a balance between surface and bottom stresses and the pressure gradient. Csanady (1973) described the wind-driven circulation in a long channel with variable depth and this work was extended by others (Wong, 1994; Matheieu et al., 2002; Hearn et al., 1987)) to study wind-driven circulation in coastal estuaries. Fischer (1976) studied the rotational current caused by a wind blowing over a variable depth channel. He observed the topographic gyres using dye plumes and concluded that wind stress exerted on coastal estuaries with variable depth can induce transverse circulation similar to topographic gyres seen in lakes (Csanady, 1973).

The freshwater flowing into an estuary at its head interacts with the salinity intrusion at the mouth of the estuary to generate a longitudinal density gradient. A net seaward flow at the surface and landward flow at the bottom due to the longitudinal density gradient is termed gravitational circulation and was described by Pritchard (1956) and Hansen and Rattray (1965) for rectangular channels. Fischer (1972) computed gravitational circulation in non-rectangular cross sections and showed that currents were landward in the deep channels and seaward in the shallow shoals. Wong (1994) derived an analytical expression for density driven gravitational circulation in an estuary with triangular cross-section and showed that the gravitational currents flowed up-estuary in the deep channel and down estuary in the shallow channel. The flow reversal with a surface down-estuary flow and bottom up-estuary flow seen in rectangular cross sections is confined to a very limited region in triangular cross sections. Thus, the vertical structure of the currents in rectangular and non-rectangular cross sections due to a down-estuary density gradient is similar to that due to down-estuary wind.

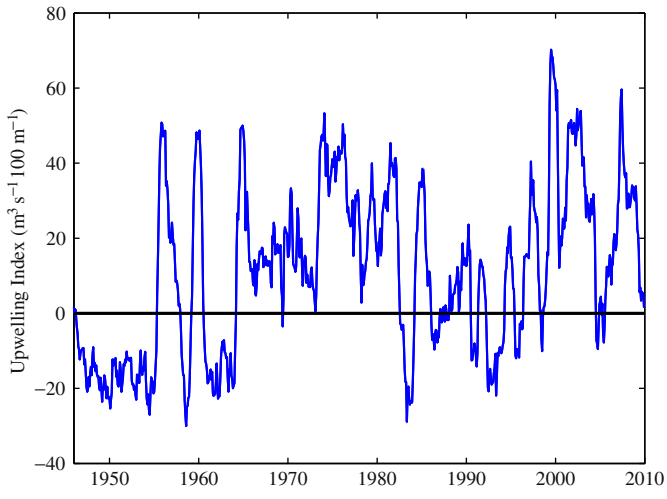

Fig. 2. 12-month running average of the upwelling index (PFEL, 2013) offshore of San Francisco Bay.

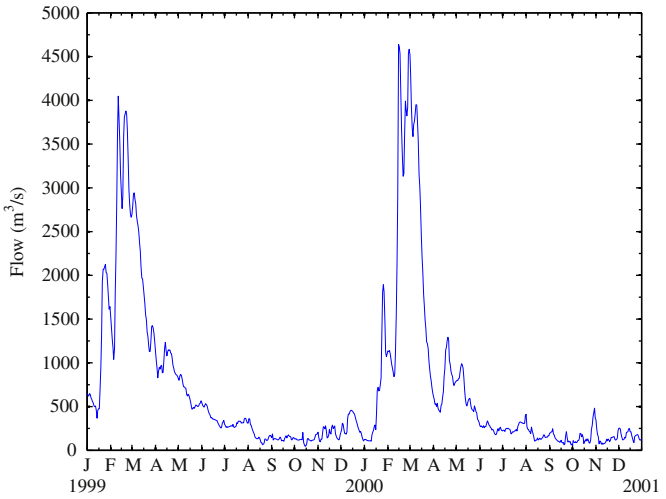

Fig. 3. Delta outflow into San Francisco Bay during 1999–2000 (DWR, 2013).

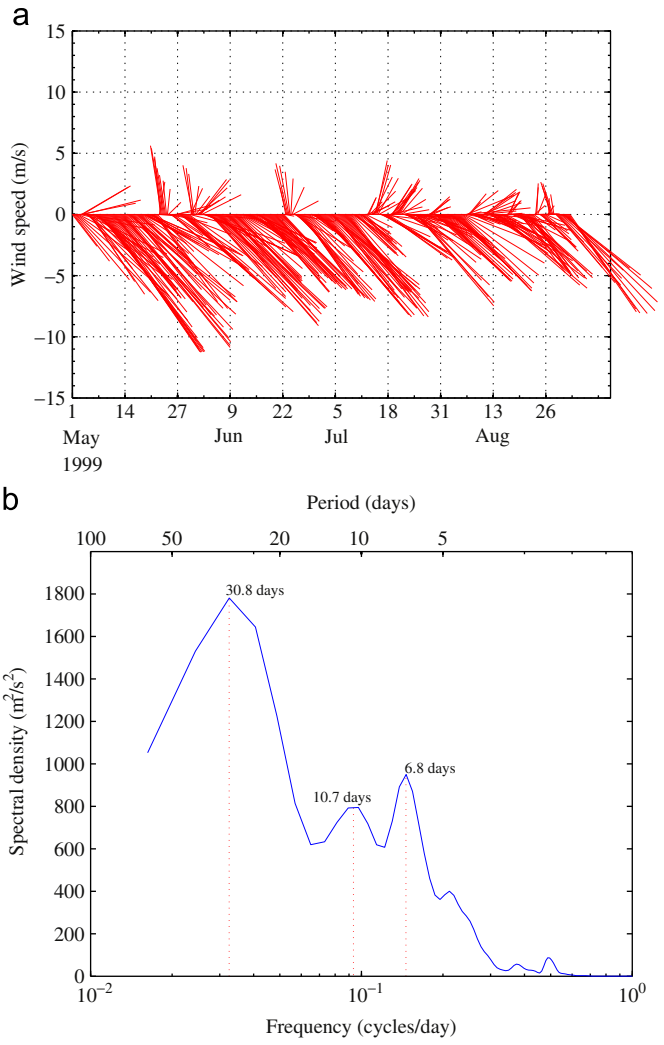

Fig. 4. (a) 40-hour low-passed winds at NDBC Buoy 46026 during the 1999 upwelling season and (b) alongshore wind spectrum with significant peaks indicated.

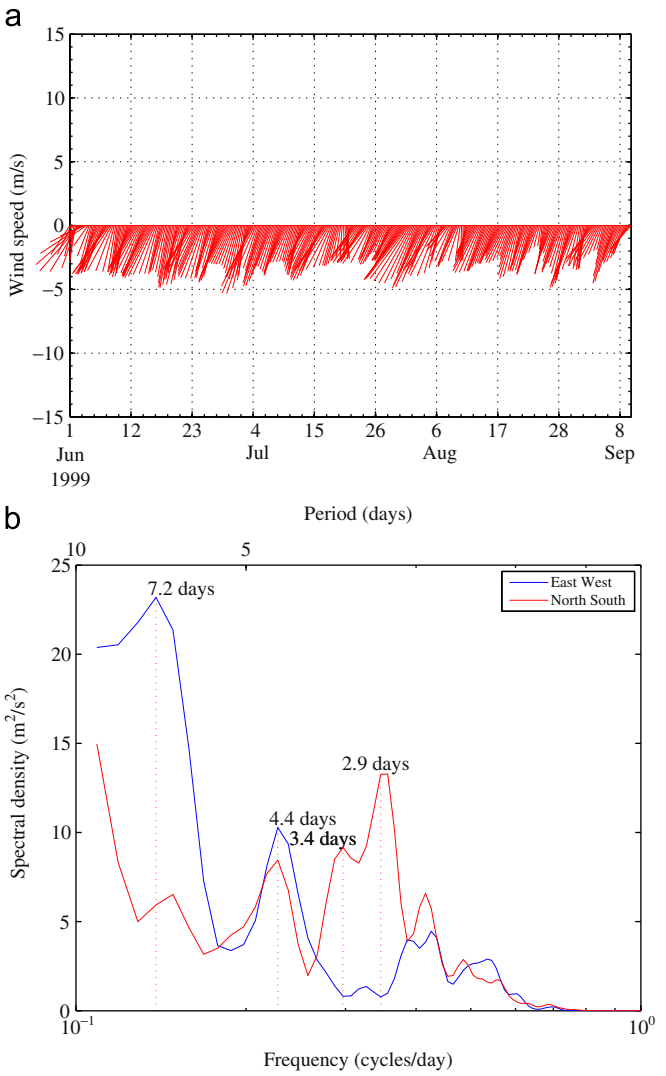

Fig. 5. (a) 40-hour low-passed winds in San Francisco Bay during the 1999 upwelling season and (b) alongshore wind spectrum with the spectral peaks indicated.

Fortnightly tides can be generated by the spring-neap variation of the bottom stresses caused by variations in tidal velocities. LeBlond (1979) showed through scaling arguments that the fortnightly tides in shallow rivers are generated due to the fortnightly modulation of the frictional forces. Ryan and Noble (2007) noted that a majority of low-frequency sea level fluctuations in San Francisco Bay that are not related to the coastal sea level fluctuations are due to the tidally induced fortnightly and monthly fluctuations. The beating of frequencies between tidal constituents O_1 and K_1 (13.66 days), M_2 and S_2 (14.77 days), and M_2 and N_2 (27.55 days) results in most commonly seen low-frequency tides in estuaries (Joseph et al., 2009; Gallo and Vinzon, 2005).

The present study seeks to understand the low-frequency fluctuations in upwelling-dominated estuaries and relate them to the forcing functions. We study San Francisco Bay because of the availability of a wealth of oceanographic and meteorological observations during the 1999 upwelling season, which had the strongest upwelling for the 60-year period, 1950–2010. Because the upwelling period in San Francisco Bay occurs during the summer months which are characterized by persistent southward winds and weak freshwater flow into the Bay, we focus on the barotropic low-frequency fluctuations. Although Walters (1982) studied the low-frequency fluctuations in currents in San Francisco Bay obtained from current meter measurements at two to three points in the water column, we study ADCP observations which give a better description of currents throughout the water column. Principal component analysis is used to distinguish the uncorrelated components in the observed low-frequency water levels and currents. We also use the SUNTANS model (Fringer et al., 2006) for San Francisco Bay described in Chua and Fringer (2011) to relate the different forcing functions to the barotropic low-frequency fluctuations in the Bay.

2. Study area

San Francisco Bay is the largest coastal embayment on the Pacific coast of United States. Fig. 1 shows a detail of the San Francisco Bay study area along with the bathymetry with typical depths ranging from 10 to 35 m in narrow channels and broad shoals with depths less than 10 m. The bathymetric data were obtained from the National Geophysical Data Center Database (NGDC, 2013) derived from US National Ocean Service (NOS) soundings in San Francisco Bay and coastal ocean. The average depth of the Bay is 6 m at mean lower low water (MLLW) and the deepest section of the main channel is at the Golden Gate, where the depth is 110 m. The prevailing winds in San Francisco Bay area are from the west and north-west. San Francisco Bay receives 90% of its freshwater inflow through the Delta at its eastern boundary and 10% of the flow from drainage and industrial discharges (Conomos et al., 1985). This freshwater flow varies seasonally with peak flows during winter storms and much reduced flows during summer and fall.

The hydrodynamic circulation in San Francisco Bay is driven by Pacific Ocean tides that propagate through the narrow opening at the Golden Gate. Tides in San Francisco Bay are characterized by differing heights in high and low tides, termed as mixed semi-diurnal tide. Walters et al. (1985) noted that the tidal wave is partially progressive in the northern reach of San Francisco Bay, while the wave is a standing wave in South San Francisco Bay. The northern reach of the Bay is characterized as a partially to well-mixed estuary with substantial longitudinal density gradients (Walters et al., 1985). South Bay is characterized as a well-mixed estuary for most of the year, except during episodic events (Cheng et al., 1993).

The 12-month moving-averaged anomalies of upwelling index offshore of San Francisco Bay are shown in Fig. 2 which shows increased upwelling intensity and its seasonal variability since 1999. The upwelling intensity offshore of San Francisco Bay is calculated by averaging the upwelling indices given by Pacific Fisheries Environmental Laboratory (PFEL) at 36°N, 122°W, and 39°N, 126°W. PFEL (2013) defines the upwelling index as the offshore component of the Ekman transport computed using the mean atmospheric pressure fields on a 3° mesh, provided by US Navy Fleet Numerical, Meteorological and Oceanographic Center (FNMOC).

Fig. 3 shows the seasonal variation of freshwater flow from the Sacramento–San-Joaquin River into the Bay during 1999–2000, obtained from the Department of Water Resources, CA (DWR, 2013). The annual mean flow into San Francisco Bay is 600 $m^3\ s^{-1}$ (Conomos et al., 1985). The freshwater flow into the Bay decreases from about 800 $m^3\ s^{-1}$ during early summer to about 300 $m^3\ s^{-1}$ during June–July. The flow rate then decreases to about 100 $m^3\ s^{-1}$ during July–August and remains at that rate at the beginning of the winter season. Fig. 4(a) shows the 40-hour low-passed winds at the National Data Buoy Center (NDBC) site 46026 during the 1999 upwelling season with a strong south-eastward wind. The observed winds are rotated in the direction of maximum variance to obtain the winds in the alongshore direction for observed winds used in this study (Emery and Thomson, 2001). Fig. 4(b) shows a power spectrum of the alongshore winds from site 46026 with distinct peaks at 6.8 and and 10.7 days. Fig. 5(a) shows the 40 hour low-passed winds at a buoy

in the Bay near San Francisco with persistent southwestward winds. Fig. 5(b) shows a power spectrum of the east-west winds at the San Francisco Buoy with peaks at 4.4 and 7.2 days, while the north–south winds show peaks around 2.9, 3.4 and 4.4 days, differing from the spectral peaks seen for the spectrum at site 46026. Wind observations in Richmond (North Bay), Alameda and Redwood City (South Bay) and San Francisco (Central Bay) were spatially well correlated in the diurnal band, but poorly correlated in the synoptic band (2–10 days). It should be noted that wind observations at San Francisco were from a buoy in the Bay, while the other wind observation stations were located close to the land and hence influenced by urban effects.

3. Analysis of low-frequency fluctuations in San Francisco Bay

High-frequency fluctuations in hourly observations of water surface elevations, currents, and winds available during June–October 1999 are removed using a 40-hour, fifth-order Butterworth low-pass filter (Emery and Thomson, 2001). Power spectral estimates for the observed surface elevations and currents were obtained using a 1024-hour Hanning window with a 50% overlap (Emery and Thomson, 2001). Principal component analysis (PCA) is used to represent the 40-hour low-passed observations with a set of uncorrelated components. The amount of variance in each principal component (PC) can be quantified by its eigenvalue.

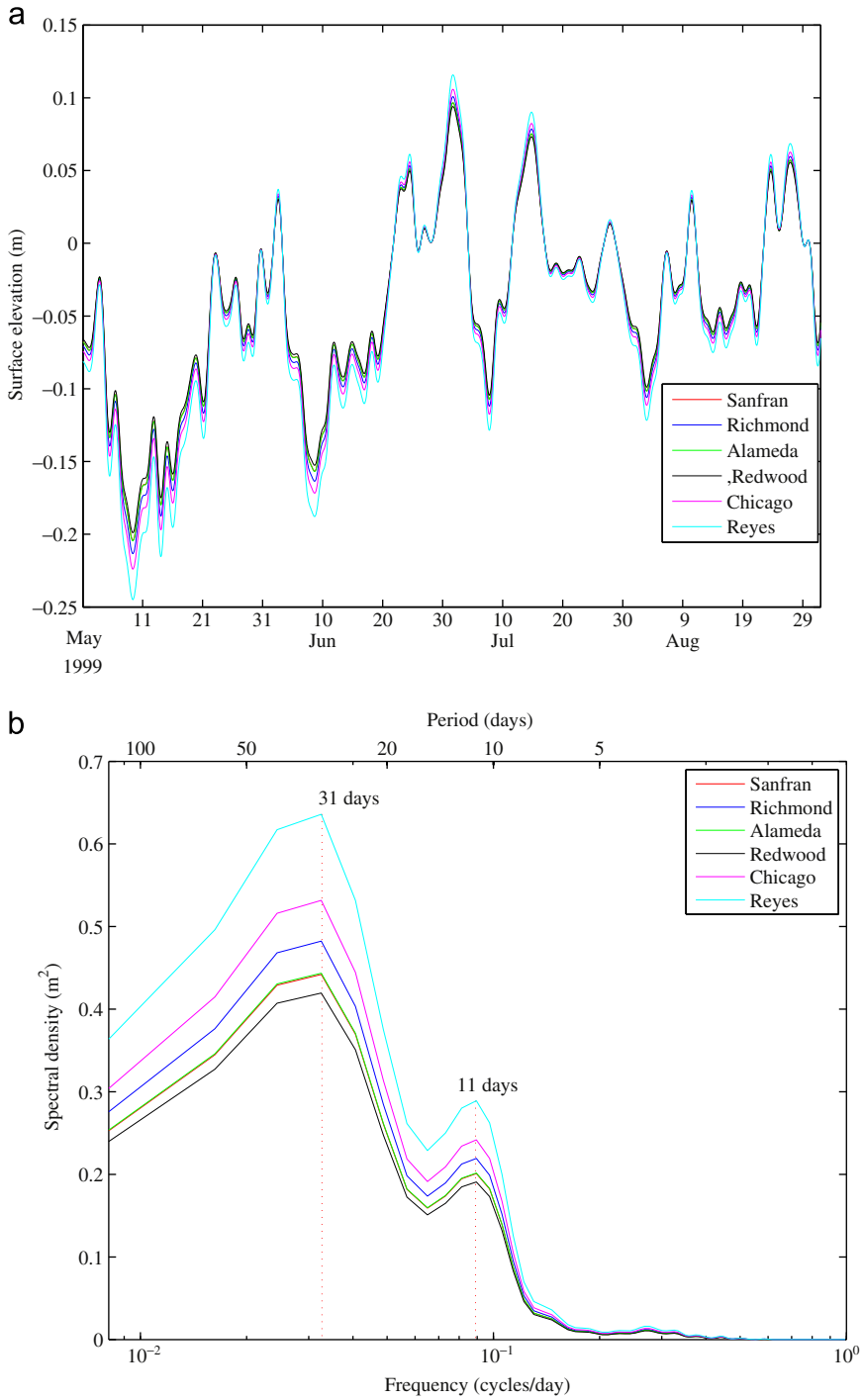

Fig. 6. (a) Surface elevations in San Francisco Bay due to the first mode during the 1999 upwelling season and (b) spectra of surface elevations due to the first mode with important peaks indicated.

Stacey et al. (2001) give a detailed procedure for determining PCA from a time series of ADCP current measurements. More details about PCA can be found in Wilks (2006) and Preisendorfer (1988). Three PC analyses have been performed in this study, one for observed surface elevations, one for observed ADCP currents at Richmond, and one for observed ADCP currents at Oakland. Harmonic analysis of observed surface elevations and currents reported in this study is performed using T_TIDE described in Pawlowicz et al. (2002).

3.1. Surface elevations

Water surface elevations are obtained at NOAA tide gauges at San Francisco, Richmond, Alameda, Redwood City, and Port Chicago. The first, second and third PCs account for 94%, 5%, and 0.4% respectively, of the variance in low-frequency surface elevations in San Francisco Bay. Fig. 6(a) shows that the surface elevations in the Bay due to the first PC co-oscillate with the coastal sea levels at Point Reyes. The lowering of the coastal sea-level on the shelf due to the offshore Ekman transport caused by southward winds is seen at all the stations in San Francisco Bay and Point Reyes. Fig. 6(b) shows the power spectrum of surface elevations for the first PC with spectral peaks at 11.2 and 30.5 days, which correspond to the spectral peaks in the offshore wind records at the NDBC site (Fig. 4(b)). Thus, the observed low-frequency water level for the first PC is primarily due to the coastal forcing at the entrance to the estuary (Ryan and Noble, 2007). The dominance of the remote forcing over local wind forcing in the low-frequency surface elevations in estuaries arises when the length of the estuary is short relative to the long wavelength of the low-frequency offshore signal (Garvine, 1985). Assuming the length of San Francisco Bay is roughly 100 km and the mean depth is 6 m, this gives a celerity of the long gravity wave of 7.67 m/s, and hence the wavelength for a 5-day period wave is 3313 km, which is one order of magnitude larger than the tidal wavelength of 343 km for the M_2 tide. This is consistent with other works which show that the wind stress along the shelf is more effective than direct wind stress in generating low-frequency sea-level fluctuations within the Bay (Garvine, 1985; Walters, 1982; Wang et al., 1997).

Unlike the first PC, the surface elevations for the second PC account for just 5% of the variance in the low-frequency fluctuations. The surface elevations due to the second PC at Port Chicago are 180° out of phase with respect to other stations in South and Central Bays

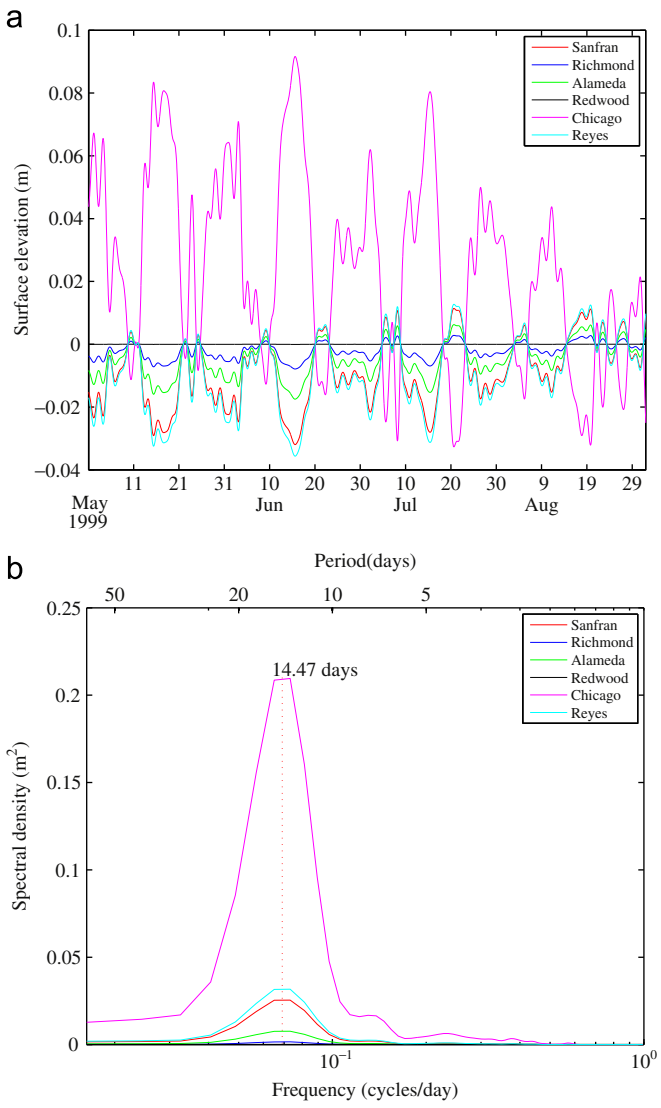

Fig. 7. (a) Surface elevations in San Francisco Bay due to the second mode during the 1999 upwelling season and (b) spectra of surface elevations due to the second mode.

Table 1
Major diurnal and semi-diurnal tidal constituents at San Francisco (NOAA).

Tidal constituent	Frequency (cycles/day)	Period (days)	Amplitude (m)	Local phase (deg)
M_2	1.9323	0.5175	0.580	338.7
S_2	2.0	0.5000	0.132	338.4
N_2	1.8960	0.5274	0.123	317.3
K_1	1.0027	0.9973	0.368	106.1
O_1	0.9295	1.0758	0.230	98.5
K_2	2.0055	0.4986	0.040	209.9

Table 2
Low-frequency tides and their periods.

Tidal constituents	Beating period (days)
M_2/S_2	14.77
K_1/O_1	13.66
M_2/N_2	27.55
M_2/S_2 and K_1/O_1	181.82

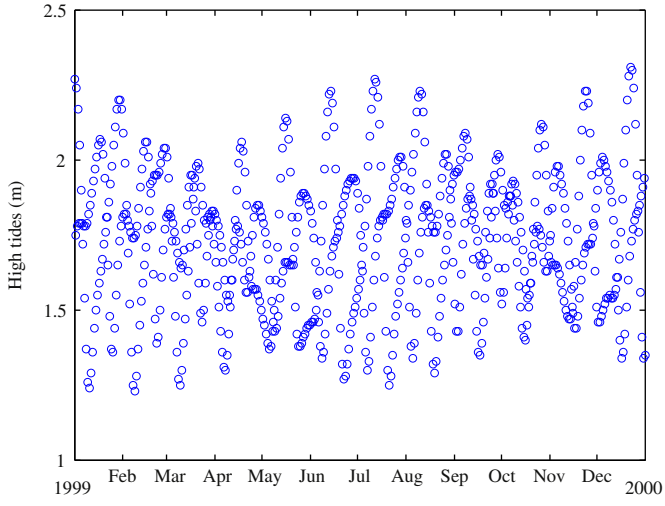

Fig. 8. Time series of high tides at San Francisco constructed from a harmonic composition of tidal constituents, showing the six-month variability arising from the interaction of the M_2/S_2 and K_1/O_1 beating frequencies.

(Fig. 7(a)) and this has been reported by Ryan and Noble (2007) in their analysis of six-year water-level records in San Francisco Bay. Fig. 7(b) shows power spectra of the water surface elevations due to the second PC with peaks at about 14 days at all stations in San Francisco Bay, but with very strong energy levels at Port Chicago, which is located in the northern reach of San Francisco Bay. A sea-level gradient between Port Chicago located at the landward end of the Bay and San Francisco at seaward end of the Bay is seen in the surface elevations (Fig. 7) for the second PC.

Table 1 gives the frequencies, amplitudes, and local phases of the major diurnal and semi-diurnal tidal constituents at the NOAA buoy at San Francisco. Table 2 gives tidal constituent pairs and their corresponding beating frequencies that give rise to the low-frequency tides. The beating period T_b in days for a beating pair with periods T_1 and T_2 in periods can be estimated (Ippen, 1966) using $T_b = T_1T_2/(T_1-T_2)$. The M_2 and S_2 tidal constituents beat to produce the Lunisolar Synodic Fortnightly (MSf) tidal constituent with a period of 14.77 days, while K_1 and O_1 beat to produce the Lunar Fortnightly (Mf) tidal constituent with a period of 13.66 days. MSf and Mf can beat to produce a constituent with a period of 180.5 days, although to the authors' knowledge this beating is interestingly not discussed in the literature. A yearly record of high tides in San Francisco Bay (Fig. 8) shows the 6-month modulation of high tides at San Francisco. NOAA (2013) tidal elevation harmonic data at San Francisco show the presence of the solar semi-annual (SSA) tidal constituent with an amplitude of 0.039 m and with a period of 182.62 days which is one half of the solar year with a period of 365.25 days. Thus, MSf/Mf beat and SSA tidal constituents are generated due to different mechanisms although their periods are close. It should be noted that peak upwelling and the semi-annual high tides both occur in July, although they are not related to one another.

3.2. Currents

Observations of currents from upward-looking ADCPs deployed by NOAA at Richmond and Oakland (Fig. 1(b)) during 1999 are used for the analysis presented in this study. The ADCP mooring at Richmond is located in the deeper part of North Bay at 15 m water depth while the ADCP at Oakland is located in the shallow part of South Bay at 10 m water depth. ADCP observations were filtered using a 40-hour low-pass filter to remove tidal and wind-induced diurnal currents. PCA is employed to decompose the observations into barotropic and baroclinic components. The observed currents are rotated in the direction of maximum variance to obtain the currents in the along- and cross-channel directions (Emery and Thomson, 2001). Harmonic analysis of the observed ADCP currents at Richmond give statistically significant amplitude estimates of the Lunisolar Synodic Fortnightly (MSf) tidal constituent, which has a period of 14.77 days (1 synodic month =29.53 days), thus confirming the presence of fortnightly tidal currents at Richmond. The MSf tidal constituent is attributed to the spring-neap variation of the tidal stresses (Joseph et al., 2009). Fig. 9 shows vertical variations in the MSf current amplitudes with a maximum current amplitude of 3 cm s^{-1} near the bottom and decreasing to a minimum amplitude of 1 cm s^{-1} near the surface. Power spectra of observed surface elevations inside the Bay for the second PC also showed a peak signal at 14.5 days (Fig. 7b). The currents due to the MSf tidal constituent are obtained by filtering the 40-hour low-passed ADCP observations using a third-order Butterworth filter with a pass band at 13–15 days. The strongest fortnightly tidal currents are seen to occur in July, which coincides with the peak upwelling season, although they are not related to one another. These fortnightly tidal currents are removed from the 40 hour low-passed ADCP observations for further analysis of the nontidal low-frequency fluctuations.

3.2.1. Observed ADCP currents at Richmond

The currents due to the MSf tidal constituent are removed by filtering out the 40-hour low-passed ADCP observations using a third-order Butterworth filter with a band-stop at 13–15 days. A PCA performed on the 40-hour low-pass filtered and 13–15 day band-stop filtered ADCP observations at Richmond shows that the

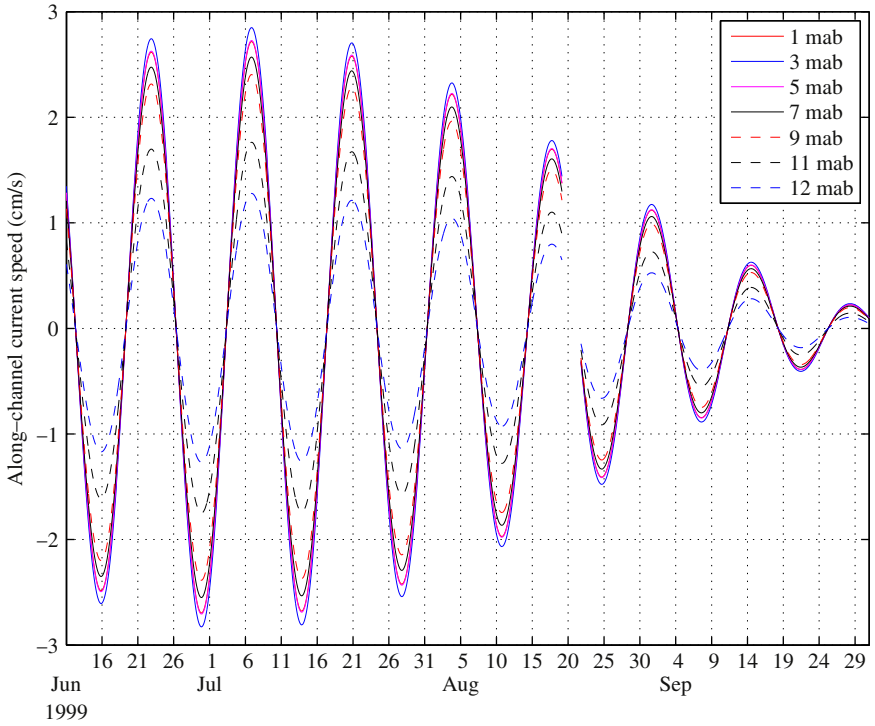

Fig. 9. Time series of low-frequency (13–15 day) along-channel tidal currents at various depths (mab—indicates m above bottom) at Richmond for the first mode during the 1999 upwelling season.

variance for the currents in the first and second PCs was 85% and 10%, respectively. Fig. 10(a) shows time series of the ADCP currents in the along-channel direction for the first PC with no significant vertical variability and current speeds ranging from 4 to 7 cm s^{-1} flowing against the direction of the prevailing winds (south-eastward) at all depths. Fig. 10(b) shows the power spectrum of along-channel currents with distinct peaks at 9 and 3.9 days, with maximum energy at mid-depth and slight decrease in energy levels towards the surface and bottom. The cross-channel currents for the first PC are generally weak (not shown) with 5% of the energy levels seen in the along-channel currents. Fig. 11(a) shows the time-averaged along-channel currents with a mean current of about 2 cm s^{-1} flowing against the direction of prevailing winds over the water column in the first PC (red line) and an estuarine flow with a seaward flow of 6 cm s^{-1} at the surface and a landward flow of 4 cm s^{-1} at the bottom in the second PC (blue line). This flow develops because the north–south pressure gradient formed due to the wind-setup dominates over the surface and bottom stress in the deeper parts of the cross-sections, generating an upwind flow. The ADCP at Richmond is located in the deeper part of the cross section and hence the observed wind-driven flow at this location is upwind. Fig. 11(b) shows time-averaged cross-channel currents (red line)

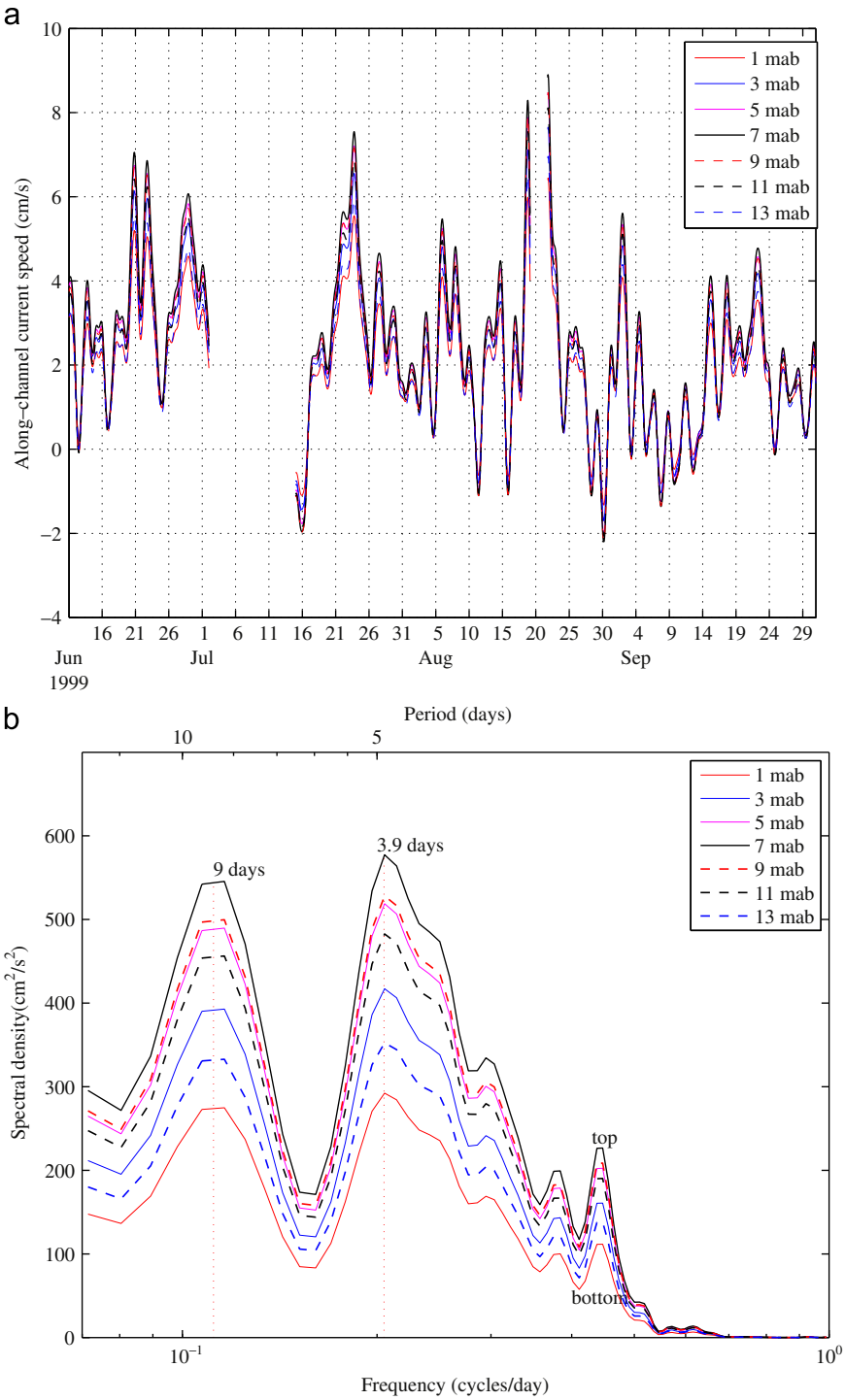

Fig. 10. (a) Time series of along-channel currents at Richmond at various depths (mab—indicates m above bottom) due to the first mode during the 1999 upwelling season and (b) associated power spectra, with important peaks indicated.

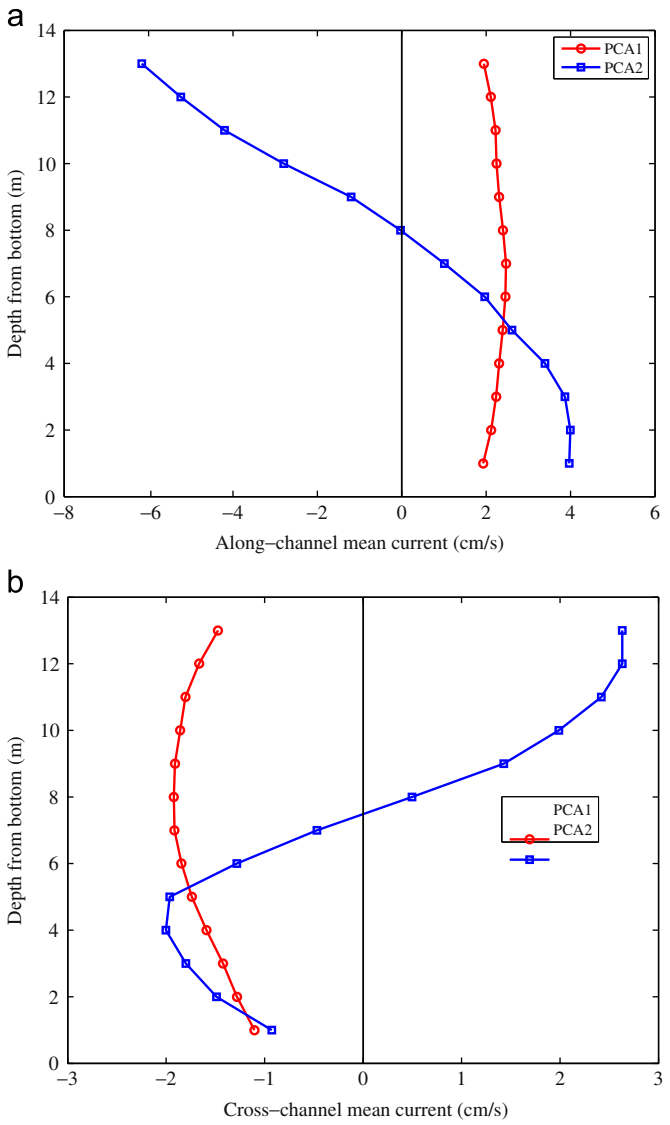

Fig. 11. Along channel (a) and cross channel (b) mean currents at Richmond during the 1999 upwelling season. Negative along-channel currents are to the south while negative cross channel currents are to the west. (For interpretation of the references to color in this figure caption, the reader is referred to the web version of this article.)

for the first PC with speeds of 1–2 cm s^{-1} throughout the water column. Time-averaged cross-channel currents for the second PC (blue line) show a two-layer estuarine circulation with a 3 cm s^{-1} eastward current near the surface and a 3 cm s^{-1} westward current near the bottom. This cross-channel baroclinic current is likely generated due to the lateral baroclinic pressure gradient between the western and eastern ends of the Bay.

3.2.2. *Observed ADCP currents at Oakland*

Harmonic analysis of ADCP observations at Oakland did not show statistically significant fortnightly MSf tidal currents in contrast to the observations at Richmond. A PCA performed on the 40-hour low-pass filtered observations at Oakland showed that the variance due to the currents in the first and second PCs were 92% and 7%, respectively. Fig. 12(a) shows time series of the along-channel observed currents due to the first PC with current speeds ranging from 2 to 14 cm s^{-1} flowing with the prevailing winds at all depths. Fig. 12(b) shows the power spectra of along-channel currents with distinct peaks at 10.2 and 6.8 days. Energy in cross-channel currents for the first PC is generally weak (not shown) with only 3% of that seen in the along-channel currents. Fig. 13(a) shows the time-averaged along-channel mean currents, for the first PC (red line) with southward speeds of 6–8 cm s^{-1} over the water column, and for the second PC (blue line) with a local estuarine current due to freshwater flows at the southern end of the Bay from streams and waste water treatment plants as hypothesized by Conomos et al. (1985). Fig. 13(b) shows the observed time-averaged cross-channel mean currents at Oakland, for the first PC (red line) to have a westward flow of 1–2 cm s^{-1} throughout the water column, and the second PC (blue line) to have a two-layer baroclinic flow in the lateral direction with 5–6 cm s^{-1} westward flow near the surface and a 3 cm s^{-1} eastward flow near the bottom. The strong cross-channel baroclinic current (Fig. 13b, red line) due to the second PC indicates that a lateral baroclinic pressure gradient could exist between the eastern and western ends of the South Bay near the ADCP location.

4. Depth-averaged model simulations of low-frequency fluctuations

The present study focuses on the barotropic circulation in San Francisco Bay and hence does not include the effects of buoyancy-driven circulation in the Bay. A two-dimensional version of the three-dimensional San Francisco Bay model of Chua and Fringer (2011) is used to understand the influence of forcing functions such as winds and coastal-forcing on the low-frequency circulation in San Francisco Bay. Chua and Fringer employed the unstructured-grid SUNTANS model of Fringer et al. (2006) in their study.

4.1. *SUNTANS model setup for San Francisco Bay*

The model grid consists of 28,539 prismatic cells and extends 40 km west from the Golden Gate into the Pacific Ocean and to the western end of the Sacramento/San-Joaquin Delta. Hourly wind records obtained from a buoy near San Francisco are used as wind forcing which is assumed constant throughout the Bay, since other wind observation stations were located close to the land and influenced by urban effects and could not be used. Observed 40-hour low-passed water levels at Point Reyes are forced along the open boundaries to examine the effects of low-frequency coastal sea levels on the Bay. The model simulations were run for a 120-day period (June–September, 1999), using a time step of 10 s. Model simulations attained a quasi-steady state after two days and hence a spin up time of seven days was used in this study. The detail of the grid near the study area is shown in Fig. 14. The bottom shear stresses are computed using the quadratic drag law, assuming a velocity profile that satisfies the log law with the roughness parameter (z_0) of 0.001 (Wang et al., 2009). For the surface wind stress, Sankaranarayanan (2005) used a quadratic drag law with a surface drag coefficient of 0.0015 for studying wind-driven circulation in New York Harbor, while Henry and Heaps (1976) used a relatively high surface drag coefficient of 0.0026 for storm surge computations in Southern Beaufort Sea. In the present study, model simulations using the quadratic drag law with a surface drag coefficient of 0.0015 gave model-predicted currents that matched well with observed currents. We ran three modeling scenarios to relate the forcing functions to the observed low-frequency fluctuations: (i) forced with winds, (ii) forced with low-frequency surface elevations, and (iii) forced with winds and low-frequency surface elevations at the Pacific Ocean boundary. No freshwater flows are imposed.

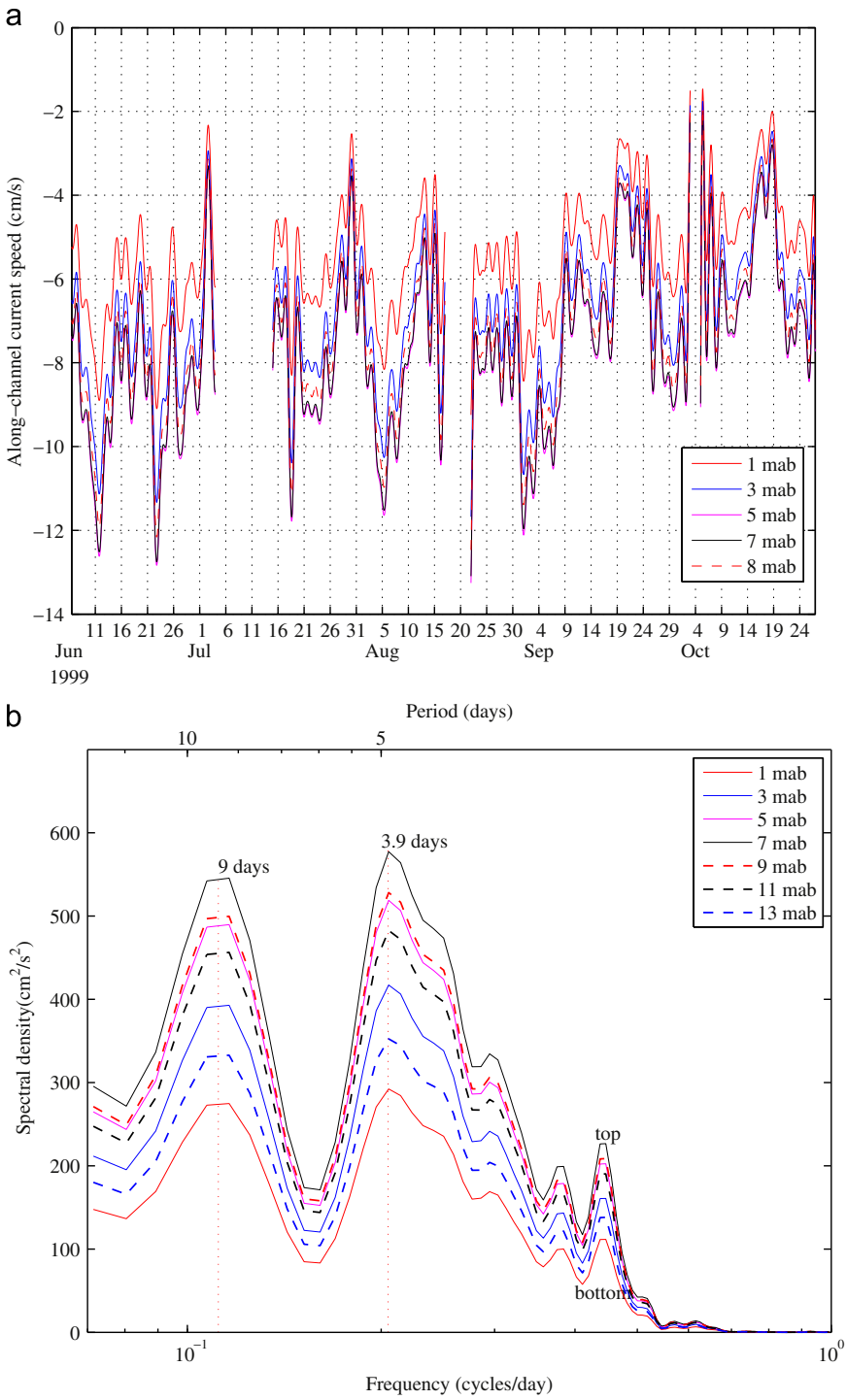

Fig. 12. (a) Time series of along-channel currents at Oakland due to the first mode during the 1999 upwelling season and (b) associated power spectra, with important peaks indicated.

4.2. *Model-predicted low-frequency sea-levels*

Model-predicted water-levels from the first scenario (forced only with winds) were filtered using a 40-hour low-pass filter to remove the diurnal variations. Fig. 15(a) shows the model-predicted low-frequency sea-levels with setdowns varying between 0.5 and 3.5 cm in the Bay. Piling up of water from the northern reaches of the Bay (Richmond) to the southern reaches of the Bay (Alameda) due to the persistent southward winds can be seen in Fig. 15(a). This north–south pressure gradient dominates over the surface and bottom shear stresses in the deeper channels and generates a flow in the upwind direction. As shown in Fig. 15(b), model-predicted water levels in the Bay from the second scenario (low-frequency water level forcing) co-oscillate with the water-levels at Point Reyes. This is consistent with the observations in Fig. 6(a) which shows that low-frequency coastal sea-levels propagate in phase throughout the Bay.

4.3. *Comparison of observed and model-predicted low-frequency currents:*

We compare the 40-hour low-passed and depth-averaged observed currents due to the first PC at the ADCP locations to

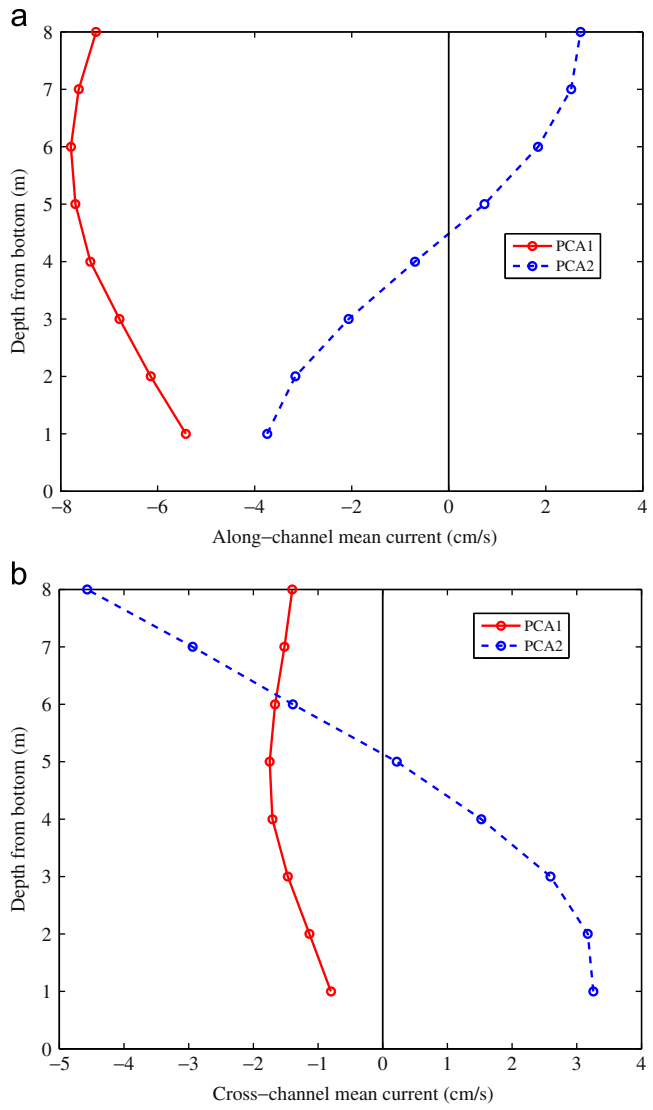

Fig. 13. Mean along channel (a) and cross-channel (b) currents at Oakland during the 1999 upwelling season. Negative along-channel currents are to the south while negative cross-channel currents are to the west. (For interpretation of the references to color in this figure caption, the reader is referred to the web version of this article.)

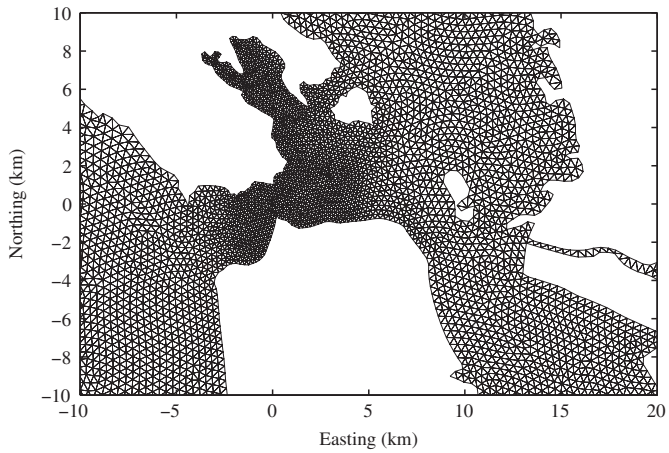

Fig. 14. Zoomed-in view of the San Francisco Bay grid employed by Chua and Fringer (2011) that is used in this study.

the barotropic depth-averaged model-predicted currents obtained with the SUNTANS model. The model-predicted 40-hour low-passed depth-averaged currents at Richmond from the first scenario (forced with winds) capture the mean upwind flow seen in the observations, as shown in Fig. 16. However, the model-predicted low-frequency currents at Richmond do not capture the 2–5 cm s^{-1} pulses that are seen in the observations.

In the second scenario, we ran the model forced with observed low-frequency water levels at Point Reyes to examine the effects of low-frequency coastal sea levels on the currents in the Bay. The model-predicted currents at Richmond due to coastal sea levels are less than 1 cm s^{-1} as shown in Fig. 16. This implies that the influence of coastal sea-levels on the currents in San Francisco Bay is small relative to the effects of local winds. This is to be expected since the coastal sea-levels propagate in phase throughout the Bay as seen from the observed low-frequency water levels due to the first PC in Fig. 6(a), leading to weak or negligible pressure gradients. In the third scenario, we ran the model forced with both observed low-frequency water levels and wind. Fig. 16 shows that model-predicted low-frequency currents at Richmond due to the combined effects of winds and low-frequency water levels were nearly the same as those due to winds alone.

Fig. 17 shows that the model-predicted 40-hour low-passed depth-averaged along-channel currents at Oakland forced with observed winds from the Buoy at San Francisco compare well with depth-averaged observed ADCP currents due to the first PC. Like the results at Richmond, the model-predicted currents at Oakland due to the 40-hour low-passed observed low-frequency sea level forced along the open boundaries are negligible. Therefore, the model predictions of depth-averaged low-frequency currents indicate that local wind forcing plays a dominant role in driving currents at Oakland. Fig. 18 compares the power spectra for the model-predicted wind-driven currents at Richmond and Oakland. These show that diurnal wind-driven currents at Richmond are stronger than at Oakland, while the currents due to the synoptic winds (2–10 days) are stronger at Oakland than at Richmond. This indicates that low-frequency winds dominate the low-frequency circulation at Oakland; but their effect is weaker at Richmond.

4.4. *Residual currents*

Residual currents in estuaries or bays are calculated by time-averaging the observed or model-predicted currents over a sufficiently long period so as to remove the oscillations due to tides and wind-driven currents (Nihoul and Ronday, 1975). Residual circulation arising from density variations is termed gravitational circulation, while the residual circulation arising from the interaction of tides with bathymetry is called tidal pumping. Most calculations of residual currents in estuaries (Cheng et al., 1993) assume that the time-dependent wind-driven currents are eliminated by averaging the currents over a long period. However, if wind blows predominantly in a particular direction as it does in San Francisco Bay during the upwelling season, residual circulation could also be caused due to winds. Cheng et al. (1993) give model estimates of residual currents due to tides although the results were not compared to observations. Walters (1982) noted that the residual currents due to the tides are relatively weak in South San Francisco Bay because of the standing wave nature of the tides there. Stacey et al. (2001) describe residual circulation patterns in North San Francisco Bay based on ADCP observations over a month during the winter of 1991. They performed a PCA of ADCP observations in Suisun Bay during the winter of 1999 and found an up-estuary residual current of 3 cm s^{-1} throughout the water column due to the first PC. However, the peak freshwater flow into the Bay during this period was 1000 m^3 s−1 and one would have expected a down-estuary residual current during the period.

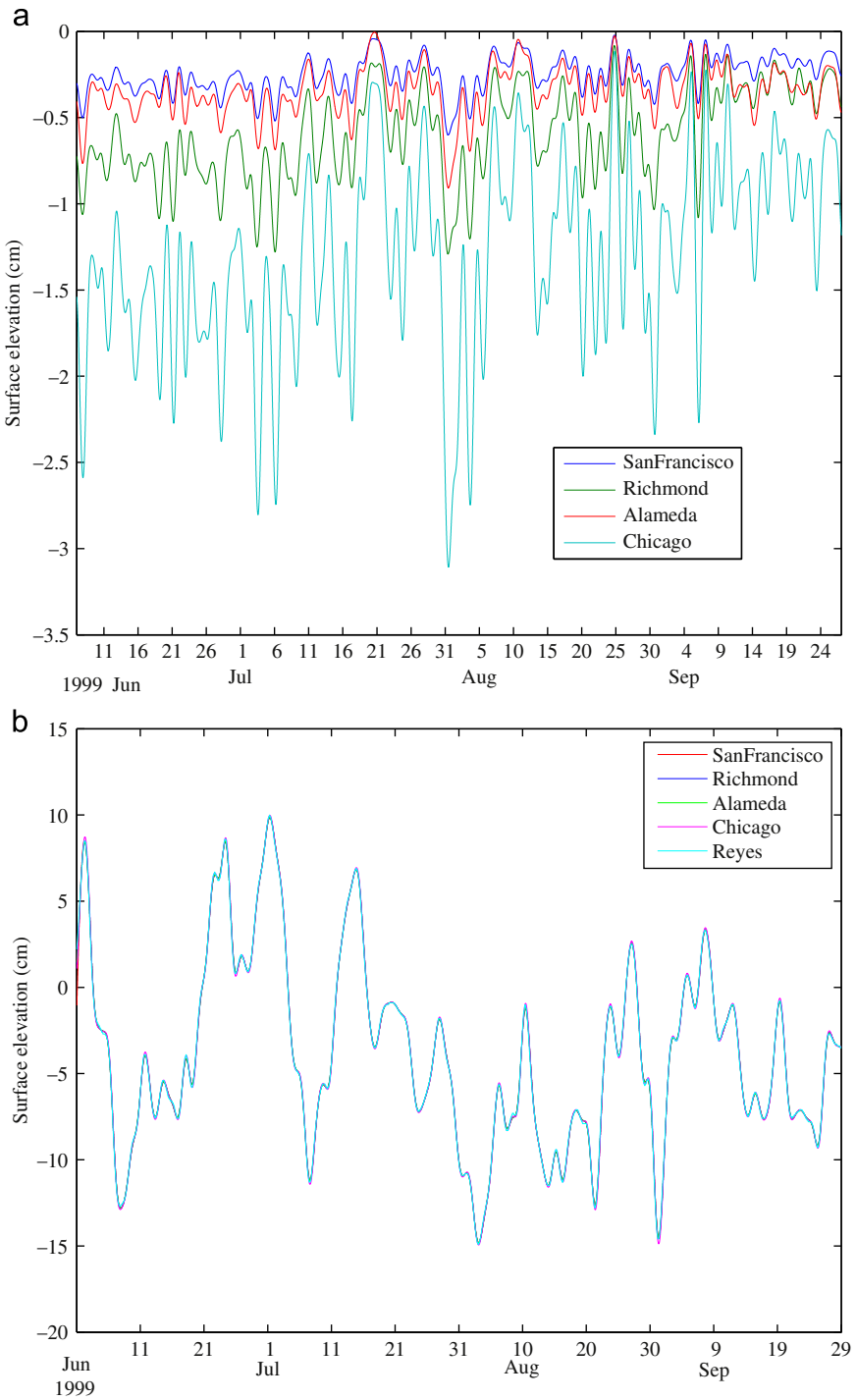

Fig. 15. Model-predicted surface elevations in San Francisco Bay (a) from scenario-1, forced by winds at the San Francisco Buoy and (b) from scenario-2, forced with 40-hour low- passed water levels at Point Reyes along the Pacific open boundary.

Stacey et al. (2001) suggested that the up-estuary residual flow seen in the observations could be due to tidal pumping or advective effects because flood tides favor the main channel and ebb tides favor a secondary small channel. However, a harmonic analysis of ADCP observations at Richmond in the present study shows a significant vertical structure in the current amplitudes of the M_2 tidal constituent with speeds of 55 cm s^{-1} near the bottom and 97 cm s^{-1} near surface (13 m from the bottom). On the other hand the observed mean current for the first PC at Richmond is 2 cm s^{-1} throughout the water column (Fig. 11(a)), flowing in a direction opposite to that of prevailing winds during the study period. Numerical model predictions forced with winds only show that the mean currents due to the first PC seen in the ADCP observations are due to winds.

4.4.1. *Residual currents due to winds*

Model-predicted depth-averaged currents at transects near the ADCP locations at Oakland and Richmond due to observed winds at San Francisco are analyzed to investigate the lateral variations in

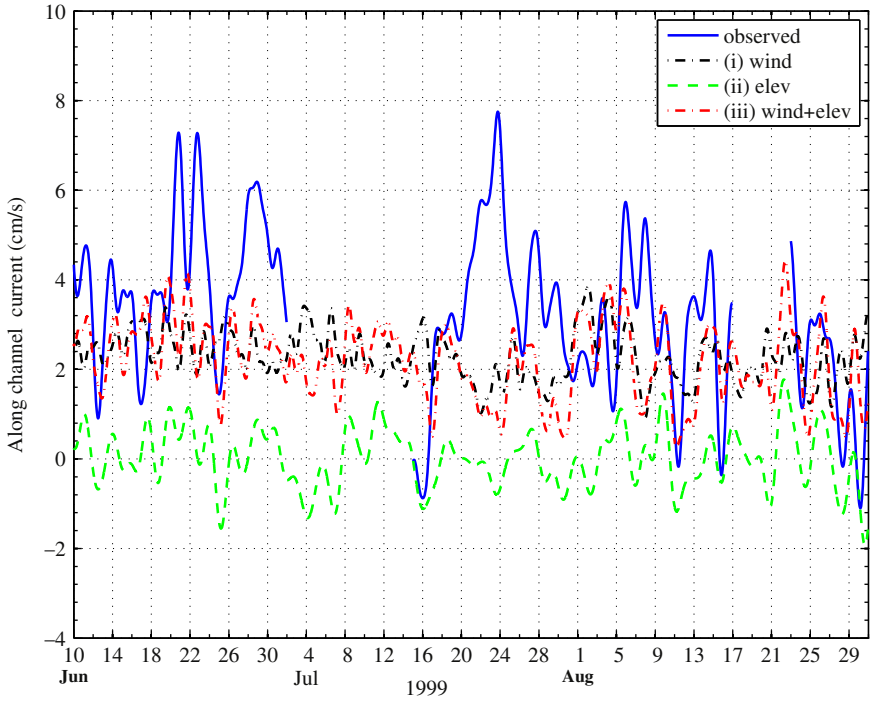

Fig. 16. Comparison of observed and model-predicted low-frequency currents at Richmond during the 1999 upwelling season for three different scenarios: (i) wind only, (ii) elevations only at the Pacific ocean boundary and (iii) wind+elevations.

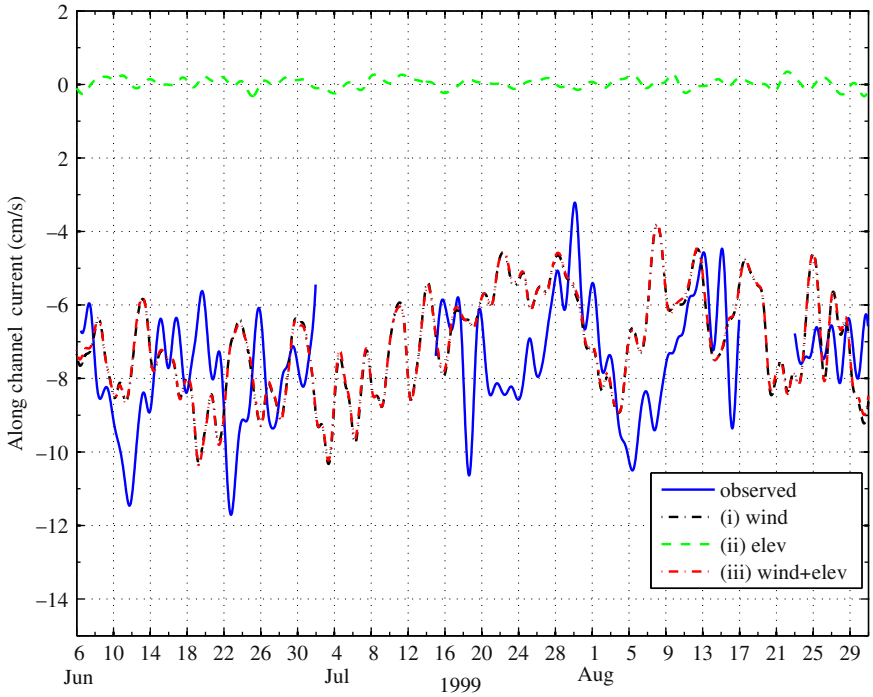

Fig. 17. Comparison of observed and model-predicted low-frequency currents at Oakland during the 1999 upwelling season for three different scenarios: (i) wind only, (ii) elevations at the Pacific Ocean boundary only and (iii) wind+elevations.

currents due to local winds. Model-predicted currents were time-averaged over the simulation period (June–September, 1999) to obtain the mean currents across the transects. Fig. 19(a and b) depict the model-predicted mean low-frequency currents at Richmond and Oakland. These show the upwind (northward) flow in the deeper regions and downwind (southward) flow in the shallow regions.

4.4.2. Currents due to steady winds

Model-simulated depth-averaged steady-state currents due to steady 6.4 m s^{-1} winds in the southwest direction in North, Central and South Bays are respectively shown in Figs. 20a–c. Steady-state currents in the direction of winds in shallow regions and upwind currents in deeper channels are seen in North, Central and South

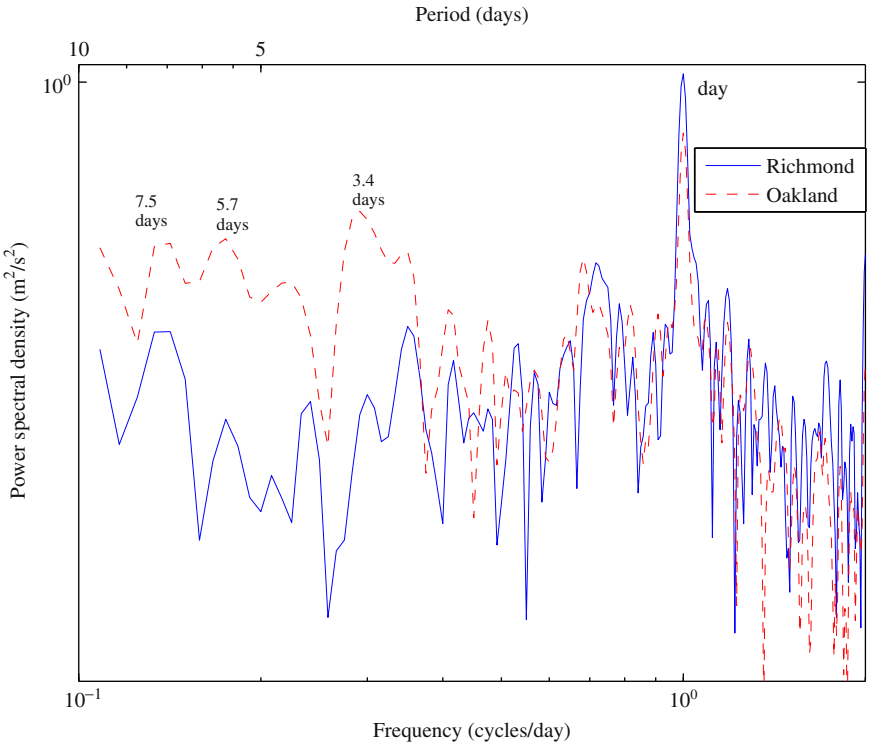

Fig. 18. Model-predicted current spectra at Richmond and Oakland due to winds only, with important peaks indicated.

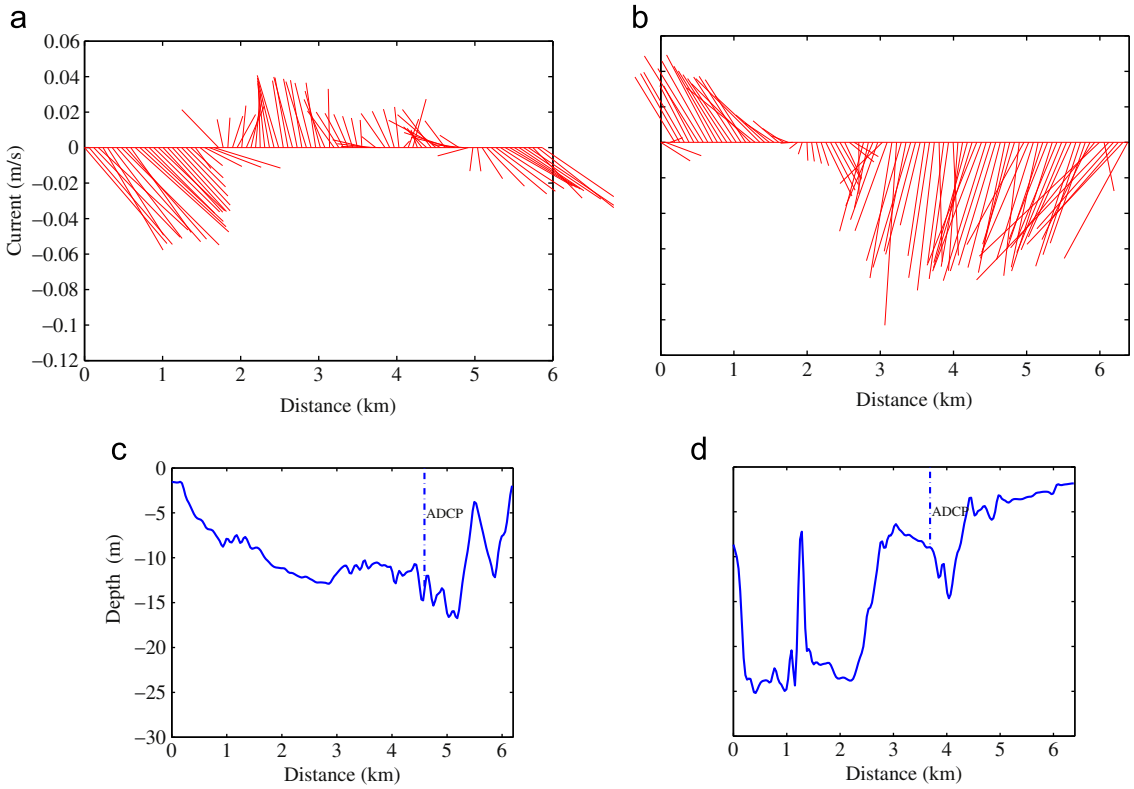

Fig. 19. Time- and depth-averaged currents due to observed winds during the 1999 upwelling season along transects through the ADCP at (a) Richmond and (b) Oakland. Bathymetry (in m relative to MSL) along the transects is shown for (c) Richmond and (d) Oakland.

Bays. Model simulations show that the winds and bathymetric variability drive transverse circulation in the Bay similar to the wind-driven topographic gyres in lakes (Csanady, 1973) and Buzzards Bay (Sankaranarayanan, 2007).

5. Summary and discussion

Three modeling scenarios, namely (i) forced with winds, (ii) forced with low-frequency surface elevations at the Pacific Ocean

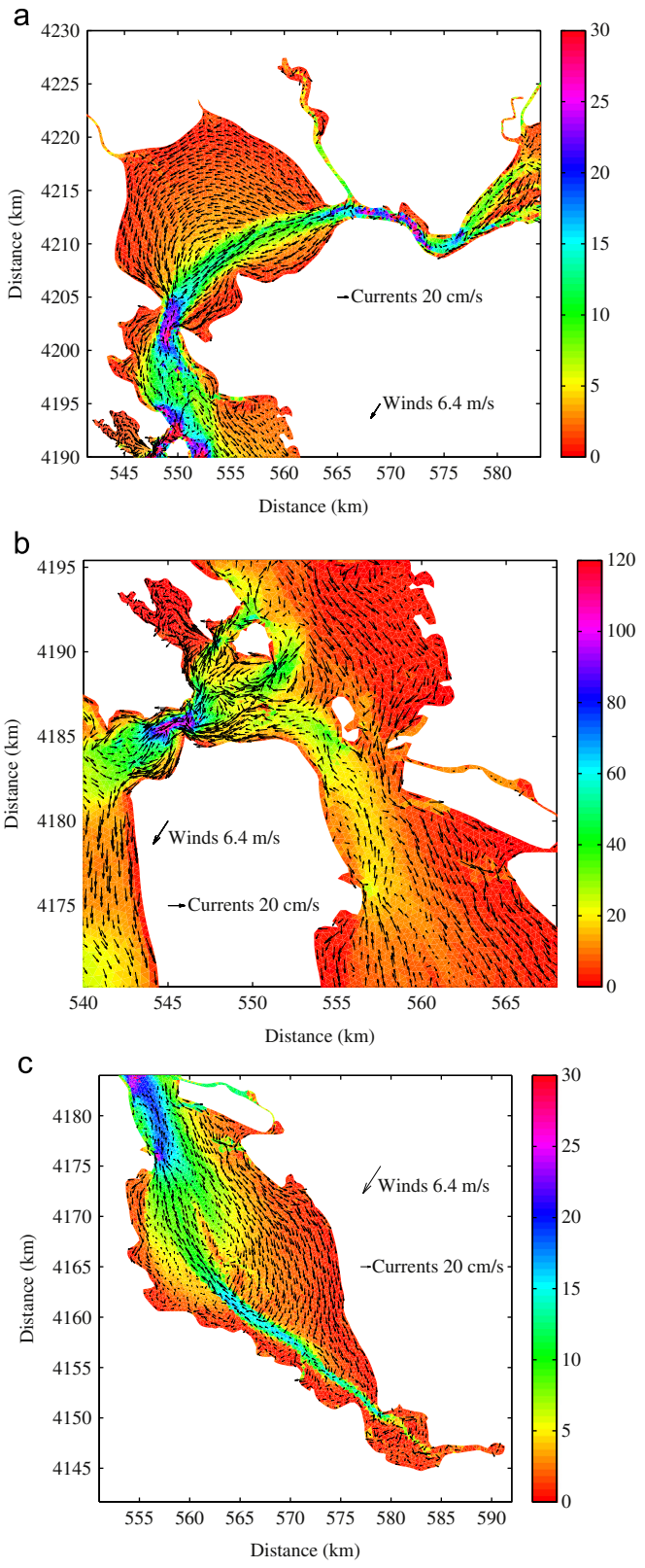

Fig. 20. Bathymetry (in m relative to MSL) and SUNTANS-predicted mean depth-averaged currents arising from a steady south-westward wind in (a) North San Francisco Bay, (b) Central San Francisco Bay and (c) South San Francisco Bay, showing how the currents in the shallow shoals flow with the wind, while the flow is against the winds in the deeper channels.

boundary, and (iii) forced with winds and low-frequency surface elevations, were run to relate the forcing in an estuary to the low-frequency fluctuations. Model simulations show that setup in water levels caused by local winds over the Bay is very small (1–3 cm) compared to the setdown at the mouth of the Bay caused by the offshore Ekman transport (roughly 1–8 cm). A significant pressure gradient is set up due to the piling of water at the southern end of the Bay due to the steady southward wind even though the height of the setup is small. Analyses of observations and model simulations show that wind stress along the shelf is more effective than direct wind stress on the Bay at generating low-frequency sea-level fluctuations within the Bay. On the other hand, the current generated due to the coastal sea level forcing at the mouth of the Bay is small because the coastal sea-level is in phase throughout the Bay and thus generates weak or negligible pressure gradients. Analyses of observed surface elevations and currents in the Bay show that the strongest fortnightly tides and tidal currents occur in July, and this coincides with the peak upwelling season, although the two processes are not related to one another.

Depth-averaged model predictions of low-frequency currents forced with observed winds show good comparison with observed low-frequency currents due to the first PC. Time- and depth-averaged model-predicted low-frequency currents at a transect through the ADCP locations at Oakland and Richmond are consistent with the linear theory that the wind-driven currents flow in the direction of the winds in the shallow parts of the cross-sections and against the winds in the deeper parts of the cross-section. The model simulations show that the observed southward currents due to the first PC are primarily due to winds.

Time series of observed currents at Richmond due to the first PC also show depth invariant fluctuations of 3–5 cm s^{-1} relative to the mean. Model-predicted low-frequency currents at Richmond forced with observed winds reproduce the mean upwind currents due to the first PC as seen in the observations but fail to capture the fluctuations. Model predictions of low-frequency currents at Richmond forced with 40-hour low passed coastal sea levels along the open boundaries were less than 1 cm s^{-1} and did not account for the fluctuations. We conclude that application of low-frequency sea level fluctuations along the offshore boundaries does not lead to improvement in the prediction of low-frequency currents in San Francisco Bay. Largier et al. (1993) observed similar very low-frequency current fluctuations on the Northern California shelf which he attributed to mesoscale eddies. The SUNTANS model outlined in this study does not take into account shelf-scale motions and a coupled bay-shelf model might be needed to capture the influence of the shelf-scale mesoscale processes in the Bay. A coupled bay-shelf model with velocities, surface elevations, salinity and temperatures obtained from the shelf model forced along the open boundaries might capture the low-frequency circulation in the Bay.

The buoyancy-driven circulation due to freshwater flow at the eastern end of the Suisun Bay and wind-driven circulation due to southward winds during the upwelling season give rise to landward flow in deeper channels and seaward flow in shallow shoals. As noted by de Velasco and Winant (2004), PCA cannot decouple two different mechanisms if the associated forcing functions lead to similar vertical structure in the currents, since the PCs are only uncorrelated. Independent component analysis (ICA) outlined in Stone (2004) produces independent components (IC) that are independent and thus help to decouple the components in the signal better than PCA. Thus ICA could be used as a follow-on project that seeks to analyze baroclinic effects on the low-frequency variability in San Francisco Bay.

Acknowledgments

We gratefully acknowledge the support of ONR Grants N00014-08-1–0904, N00014-05-1–0294, and N00014-10-1–0521 (Scientific

officers: Dr. Scott Harper, Dr. Theresa Paluszkiewicz, Dr. C. Linwood Vincent). The first author is grateful to his family for their support while this manuscript was being finalized. Many thoughtful comments from the two anonymous reviewers which helped to significantly improve the manuscript are gratefully appreciated. We also thank Vivien Chua for the San Francisco Bay grid and Bing Wang for her help with the SUNTANS model.

References

Cheng, R.T., Casulli, V., Gartner, J.W., 1993. Tidal, residual, intertidal mudflat TRIM model and its applications to San Francisco Bay. Estuarine, Coastal and Shelf Science 369, 235–280.

Chua, V., Fringer, O.B., 2011. Sensitivity analysis of three-dimensional salinity simulations in North San Francisco Bay using the unstructured-grid suntans model. Ocean Modelling 39 (3–4), 332–350.

Cloern, J.E., 1996. Phytoplankton bloom dynamics in coastal ecosystems: a review with some general lessons from sustained investigation of San Francisco Bay, California. Reviews of Geophysics 103 (2), 127–168.

Cloern, J.E., Jassby, A.D., Thompson, J.K., Keib, K., 2007. A cold phase of the East Pacific triggers new phytoplankton blooms in San Francisco Bay. Proceedings of the National Academy of Sciences of the United States of America 104 (47), 18,561–18,656.

Cloern, J.E., et al., 2010. Biological communities in San Francisco Bay track large scale climate forcing over the North Pacific. Geophysical Research Letters 37 (L21), 602.

Conomos, T.J., Smith, R.E., Gartner, J.W., 1985. Environmental setting of San Francisco Bay. Hydrobiologia 129, 1–12.

Csanady, G.T., 1973. Wind-induced barotropic motions in long lakes. Journal of Physical Oceanography 3, 429–438.

de Velasco, G.G., Winant, C.D., 2004. Wind- and density-driven circulation in a well mixed estuary. Journal of Physical Oceanography 34, 1103–1116.

DWR, ⟨http://www.water.ca.gov/dayflow/output/Output.cfm⟩, last accessed on May, 14, 2013.

Emery, W., Thomson, R.E., 2001. Data Analysis Methods in Physical Oceanography. Elsevier, New York.

Fischer, H.B., 1972. Mass transport mechanisms in partially stratified estuaries. Journal of Fluid Mechanics 53 (4), 671–687.

Fischer, H.B., 1976. Mixing and dispersion in estuaries. Annual Review of Fluid Mechanics 8, 107–113.

Fischer, H.B., List, E.J., Koh, R.C.Y., Imberger, J., Brooks, N.H., 1979. Mixing in inland and coastal waters. Academic Press, New York.

Fringer, O.B., Gerritsen, M., Street, R.L., 2006. An unstructured-grid, finite-volume, nonhydrostatic, parallel coastal ocean simulator. Ocean Modelling 14 (3), 139–173.

Gallo, M.N., Vinzon, S.B., 2005. Generation of overtides and compound tides in Amazon estuary. Ocean Dynamics 55 (5–6), 441–448.

Garvine, R.W., 1985. Simple model of estuarine subtidal fluctuations forced by local and remote stress. Journal of Geophysical Research 90 (C6), 11,945–11,948.

Hansen, D.V., Rattray, M., 1965. Gravitational circulation in straits and estuaries. Journal of Marine Research 23, 104–122.

Hearn, C.J., Hunter, J.R., Heron, M.L., 1987. The effects of a deep channel on the wind-induced flushing of a shallow bay or harbor. Journal of Geophysical Research 92 (C4), 3913–3924.

Henry, R.F., Heaps, N.S., 1976. Storm surges in the southern Beaufort Sea. Journal of the Fisheries Board of Canada 33 (10), 2362–2376.

Hickey, B.M., Banas, N.S., 2003. Oceanography of the US Pacific Northwest coastal ocean and estuaries with application to coastal ecology. Estuaries 26 (4B), 1010–1031.

Joseph, A., Balachandran, K.K., Mehra, P., Desai, R.G.P., VijayKumar, K., Agarvadekar, Y., Dabholkar, N., 2009. Amplified Msf tides at Kochi backwaters on the southwest coast of India. Current Science 97 (6), 776–784.

Ippen, A.T., 1966. Estuary and Coastline Hydrodynamics. 1966. McGraw-Hill Book Company, Inc., New York p. 762*p*.

Largier, J., 1996. Hydrodynamic exchange between san francisco bay and the ocean: the role of ocean circulation and stratification. In: Hollibaugh, T. (Ed.), San Francisco Bay: The Ecosystem. American Association for the Advancement of Science, New York, pp. 69–104.

Largier, J.L., Magnell, B.A., Winant, C.D., 1993. Subtidal circulation over the Northern California Shelf. Journal of Geophysical Research 98 (C10), 18,147–18,179.

LeBlond, P.H., 1979. Forced fortnightly tides in shallow rivers. Atmosphere–Ocean 17 (3), 253–264.

Lorenzo, E.D., et al., 2008. North Pacific Gyre Oscillation links ocean climate and ecosystem change. Geophysical Research Letters 35 (GL032), 838.

Matheieu, P.-P., Deleersnijder, E., Cushman-Roisin, B., Beckers, J.-M., Bolding, K., 2002. The role of topography in small well-mixed bays with application to the Lagoon of Mururoa. Continental Shelf Research 22, 1379–1395.

NGDC, ⟨http://maps.ngdc.noaa.gov/viewers/nos_hydro/⟩, accessed on April 14, 2013.

NOAA, ⟨http://tidesandcurrents.noaa.gov/station_retrieve.shtml?type=Harmonic+Constituents⟩ accessed on April 22, 2013.

Nihoul, J.C.J., Ronday, F.C., 1975. The influence of the "tidal stress" on the residual circulation application to the Southern Bight of the North Sea. Tellus XXVI 5, 484–489.

PFEL, ⟨http://www.pfeg.noaa.gov/products/pfel/modeled/indices/upwelling/upwelling.html⟩, last accessed on April, 13, 2013.

Pawlowicz, R., Beardsley, B., Lentz, S., 2002. Classical tidal harmonic analysis including error estimates in MATLAB using T_TIDE. Computers & Geosciences 28 (8), 929–937.

Preisendorfer, R.W., 1988. Principal Component Analysis in Meteorology and Oceanography. Elsevier, New York.

Pritchard, D.W., 1956. The dynammic structure of a coastal plain estuary. Journal of Marine Research 15, 3–42.

Ryan, H.F., Noble, M.A., 2007. Seasonal sea-level variations in Central California at subtidal to decadal and longer time scales with implications for San Francisco Bay, California. Estuarine, Coastal and Shelf Science 73, 538–550.

Sankaranarayanan, S., 2005. A 3D boundary-fitted barotropic hydrodynamic model for the New York Harbor region. Continental Shelf Research 25 (18), 2233–2260.

Sankaranarayanan, S., 2007. Modeling the tide and wind-induced circulation in Buzzards Bay. Estuarine, Coastal and Shelf Science 73 (3), 467–480.

Stacey, M.T., Burau, J.R., Monismith, S.G., 2001. Creation of residual flows in a partially stratified estuary. Journal of Geophysical Research 103 (17), 013–17,037.

Stone, J.V., 2004. Independent Component Analysis: A Tutorial Introduction. The MIT Press.

Walters, R.A., 1982. Low-frequency variations in sea level and currents in South San Francisco Bay. Journal of Physical Oceanography 12, 658–668.

Walters, R.A., Cheng, R.T., Conomos, T.J., 1985. Time scales of circulation and mixing processes of San Francisco Bay waters. Hydrobiologia 129, 13–36.

Wang, B., Fringer, O.B., Giddings, S.N., Fong, D.A., 2009. High-resolution simulations of a macrotidal estuary using SUNTANS. Ocean Modelling 26 (1–2), 60–85.

Wang, D.-P., Elliot, A.J., 1978. Non-tidal variability in Chesapeake Bay and Potomac River: evidence for non-local forcing. Journal of Physical Oceanography 8 (2), 225–232.

Wang, J., Cheng, R.T., Smith, C., 1997. Seasonal sea-level variations in San Francisco Bay in response to atmospheric forcing, 1980. Estuarine, Coastal and Shelf Science 45, 39–52.

Wilks, D.S., 2006. Statistical Methods in the Atmospheric Sciences. Academic Press.

Wong, K.-C., 1994. On the nature of transverse variability in a coastal plain estuary. Journal of Geophysical Research 99 (C7), 14,209–14,222.

Wong, K.-C., Wilson, R.E., 1984. Observations of low-frequency variability in Great South Bay and relations to atmospheric forcing. Journal of Physical Oceanography 14, 1893–1900.